Experimental Investigation of Deformation in 5083 Marine-Grade Aluminum Alloy at Elevated Temperatures

Basil M. Darras, Farid H. Abed, Akrum Abdul-Latif, and Salman Pervaiz

This paper presents an experimental study to investigate the thermo-mechanical behavior of marine-grade aluminum alloy (AA5083) under quasi-static loading. A series of tensile tests were conducted to generate the true stress-true strain curves at a range of initial temperatures between 25 and 350 °C and at low to intermediate strain rates of 0.001 and 0.1 s^{-1}; respectively. The coupling effect of temperature and strain rate on the flow stress of AA5083 was more pronounced at elevated temperatures. Microhardness tests were also conducted at 1 cm intervals along the gage length. Consistent relationships between the fracture strength of the specimens and their microhardness profiles were observed. Scanning electron microscopy (SEM) coupled with image analysis techniques was used to characterize the internal damage at fracture. The size and area of void growth and coalescence were obtained and SEM results showed that void fraction increases with temperatures and accumulation of plastic strain.

1. Introduction

Several materials such as 5083 aluminum alloy have been used in various industrial sectors (e.g., shipbuilding, different vehicles and truck bodies, pressure vessels, etc.) due to their appropriate mechanical properties. Such industrial applications may involve large deformation including shear localizations and internal damages due to impact and other types of loadings. Investigation of local phenomena within materials requires a particular attention to develop constitutive equations capable of describing correctly their non-linear plastic (or viscoplastic) behavior coupled with damage (Ref 1–5).

Aluminum alloy 5083 has a moderate strength, a good corrosion resistance, and an excellent low temperature superplasticity. It is important to emphasize that superplastic flow is terminated by an internal cavitation process leading to voids coalescence to final fracture (Ref 6–8). Cavities nucleate at the matrix-particle interface (precipitations identified as Al3Cr, Al3Zr, and Al6Mn) (Ref 9). Bae and Ghosh showed that the recrystallization process cannot totally eliminate the damage at the particle interface (Ref 10). These are the nucleation sites for cavities during deformation. It has been shown that the size of intermetallic particles in the alloy exerts a significant influence on the recrystallization process (Ref 11). Annealing is predominantly controlled by continuous recrystallization in the hot working of aluminum alloy 5083. Dynamic recrystallization leads to the superplastic behavior of the AA5083 (Ref 12).

Several researchers have investigated the deformation of aluminum alloys by studying the effects of different loading conditions, strain rates, alloying elements, heat treatment conditions, and temperature (e.g., Ref 13–17). El-Danaf et al. studied the effect of temperature and strain rate on the deformation of Ca-modified AA5083 (Ref 13). Temperature and strain rate ranges from 573 to 723 K and from 10^{-5} to 10^{-1} s^{-1} were discussed in their study. Cleveland et al. studied the superplastic behavior of two 5083 aluminum alloys with slight differences in compositions and strain rate sensitivity (Ref 15). The results pointed out a change in strain rate sensitivity and the concentration of cavity causing particles affecting the superplastic behavior of the alloy. Tucker et al. studied the effect of stress states and strain rates on plasticity, damage evolution, and fracture in three different aluminum alloys (Ref 14). Several deformation paths at different strain rates were considered. Their results suggested that flow stress and damage evolution are more sensitive to stress states rather than strain rate. Iwasaki et al. investigated the effect of temperature on the flow stress of superplastic commercial 5083 aluminum alloy (Ref 16). They presented a constitutive equation for this alloy based on the Dorn equation.

From modeling perspective, ductile damage due to micro-voids evolution occurs especially in plastically localized zones where the stress triaxiality is high. The latter stress state has a significant effect on void growth and its rate. Void initiation and growth have been extensively studied by means of micro-mechanics analysis by several authors. Gurson proposed a damage model based on continuum theory of ductile rupture by void nucleation and growth for porous perfectly plastic matrix (Ref 18). Due to its limitations, several extensions have been made [e.g., Ref 19–22).

This paper examines the effect of temperature and strain rate on deformation and damage evolution of 5083 marine-grade aluminum alloy. The main goal is to provide a better understanding of the thermo-mechanical response of AA5083 which may later help develop a coupled damage-plasticity constitutive model for large deformation. A range of initial temperatures 25, 200, 275, and 350 °C at two quasi-static strain rates of 0.001 and 0.1 s^{-1} were investigated. Damage was

Basil M. Darras, Farid H. Abed, and **Salman Pervaiz**, College of Engineering, American University of Sharjah, Sharjah, UAE; and **AkrumAbdul-Latif**, College of Engineering, American University of Sharjah, Sharjah, UAE; and Département GIM, Université Paris 8 IUT de Tremblay-en-France, 3 rue de la Râperie, 93290 Tremblay-en-France, France. Contact e-mail: bdarras@aus.edu.

analyzed for the fractured surfaces in terms of voids area fraction and average size. And microhardness was measured along the deformed samples. The results herein indicate the importance of the temperature and strain rate coupling effect on the damage evolution leading to fracture.

2. Experimental Procedure

2.1 Specimen Material

In the present research, a commercially available 5083 aluminum alloy was selected and studied because of its high strength to weight ratio and corrosion resistance. The material was available in sheet with 4 mm thickness. The microstructure of AA5083 is mainly composed of 4.1% of magnesium (Mg), 0.66% of manganese (Mn), 0.28% of iron (Fe), 0.18% of silicon (Si), 0.1% of chromium (Cr), and 0.02% of copper (Cu), in addition to more than 94% of pure aluminum (Al).

2.2 Tensile Test Setup

Dog-bone-shaped tensile specimens with gage length of 80 mm and a cross-section of 12 mm × 4 mm were utilized for experimentation. The specimens were machined in accordance with ASTM E8-03 standards (Ref 23). Tensile tests were conducted at various temperatures (25, 200, 275, and 350 °C) and extension speeds of 5 and 500 mm/min which were equivalent to strain rates of 0.001 and 0.1 s^{-1}, respectively. The thermo-mechanical tests were conducted using an INSTRON 5582 universal testing machine surrounded by a Zwick/Roell 3-zone high temperature furnace that was independently controlled. The temperature was maintained within ±1 °C of the test temperature over the specimen gage length using universal 3-zone furnace controller (model ME44-180). The furnace was equipped with one thermocouple of Ni/CrNi in each zone. Three additional thermocouples were mounted directly to the sample. The tests were performed by placing the specimen and load train within upper and lower cover plates. After heating-up, these tests begun when the three thermocouples (located directly at the top, middle, and bottom of the specimen's gage length) gave the required temperature with a difference not exceeding ±1 °C.

2.3 Microhardness Testing

Vicker's microhardness tests were conducted using Qualitest microhardness tester (QV-1000 DM), in accordance with ASTM E348-11 (Ref 24). The test was performed using a load of 1 kg. Specimens were marked at the fracture location as a reference point and the gage length of specimen was divided into equal parts spaced 1 cm. Figure 1 shows a sample used for the microhardness test. At the cross-section of each part, microhardness measurement was repeated five times and the average values were reported. The mutual distance between neighboring sites was approximately 1 mm to avoid possible interference.

2.4 Scanning Electron Microscopy

A scanning electron microscope (SEM), TESCAN Vega3 LM series, was utilized to examine voids within the fracture zone of tensile specimens. SEM samples were cut from locations near the fracture surface and were polished prior to examination. An in-house image processing code was used to analyze and estimate void area fractions as illustrated in Fig. 2. Binary images were first obtained by identifying the different gray/black areas in the SEM images. This was done by setting a threshold pixel value such that everything below it is assumed as an air void and everything above that threshold is assumed to belong to a solid surface. The density, count, and average size of voids are then computed.

3. Results and Discussions

3.1 Stress-Strain Curves

Figure 3(a) and (b) show the true stress-true strain curves at different combinations of strain rates and temperatures. The results show that a maximum strain of 1.0 was achieved at the combination of lowest strain rate of 0.001 s^{-1} and the highest temperature of 350 °C, which suggests that this alloy behaves superplastically within that range. The effect of strain rate and temperature on the tensile behavior of the material is clearly illustrated. Increasing temperature tends to increase the ductility of the material while reducing the strength of the material. Increasing the strain rate has an opposite effect. At low temperature, AA5083 shows low sensitivity to strain rate; however, when the temperature was increased the effect of the strain rate became more significant.

Hardening moduli as function of the true strain were also investigated as presented in Fig. 4(a) and (b). It is clear that more strain hardening has taken place at lower temperature and this is due to the fact that 5000 series of aluminum alloys exhibit significant hardening with the accumulation of plastic strain at low temperature; however, at higher temperature, less hardening occurs in the material. When it comes to the effect of the strain rate on hardening, more strain hardening is observed at higher strain rate. Another important observation is that at higher temperature the effect of strain rate on hardening
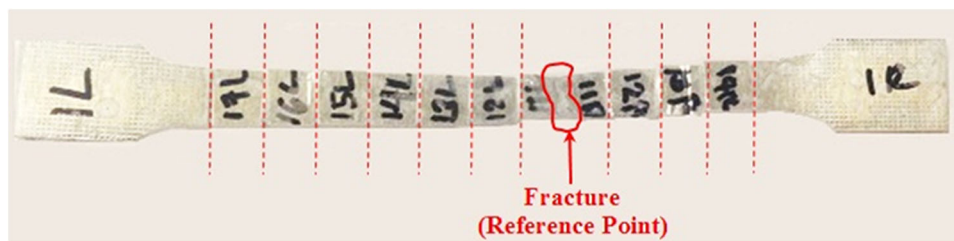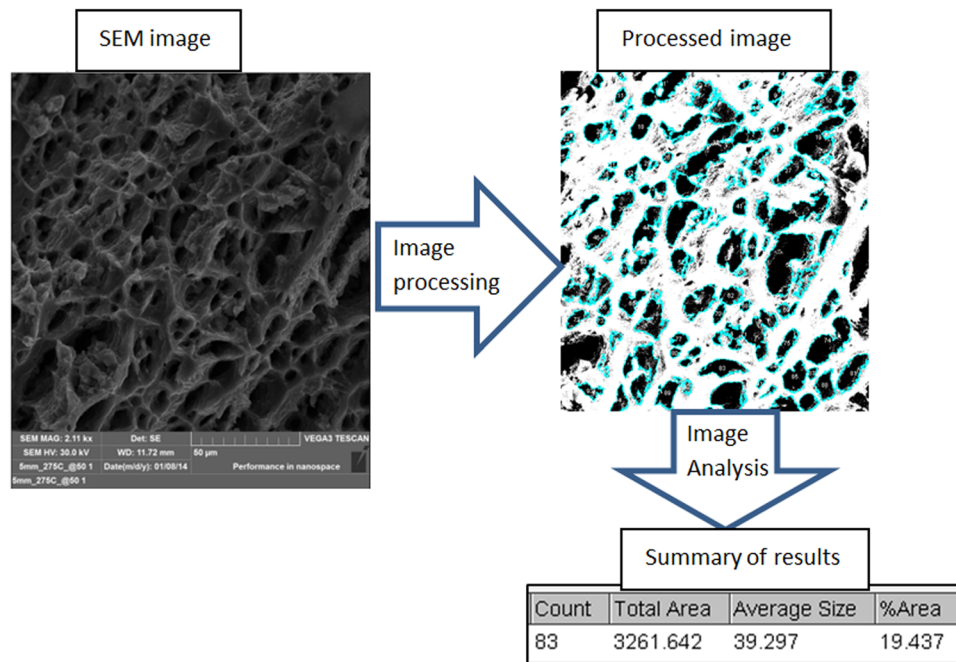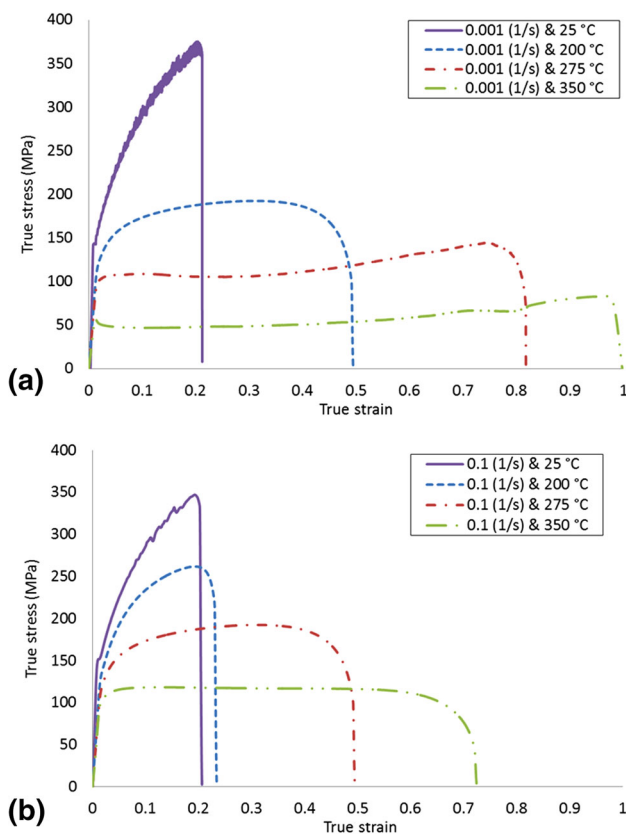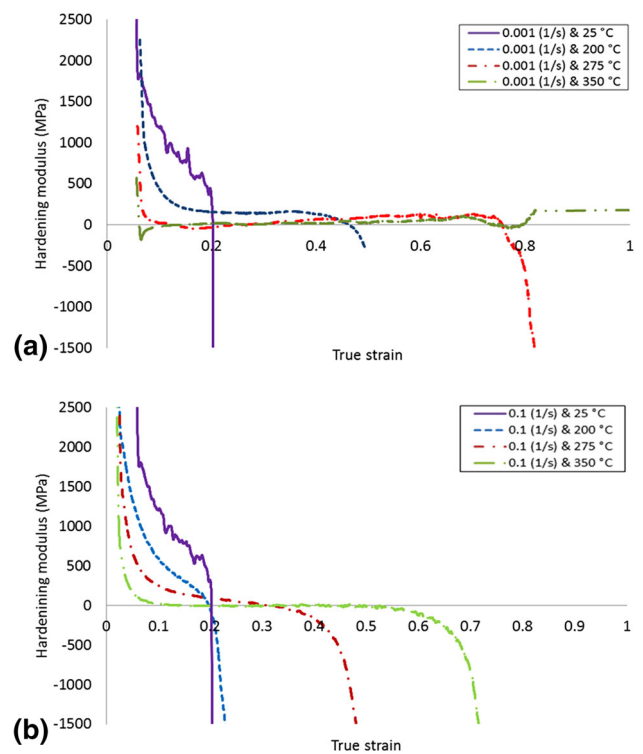

Fig. 1 Sample preparation for microhardness test

Fig. 2 Void analysis

Fig. 3 True stress-true strain curves at strain rate of (a) 0.001 s^{-1} and (b) 0.1 s^{-1}

Fig. 4 Hardening modulus at strain rate of (a) 0.001 s^{-1} and (b) 0.1 s^{-1}

modulus was not observed to the same degree as the samples tested at low temperature.

It was concluded that the rate of change of the hardening is rapid during tests at room temperature. However, this evolution decreases gradually with temperature rising. At 200 °C and a strain rate of 0.001 s^{-1}, the hardening evolves at a lower rate compared to the room temperature case up to the final failure. With further temperature increase (i.e., 275 and 350 °C), the material deforms with perfect viscoplastic behavior (without hardening) up to 30% of strain for both temperatures. Subsequently, the material reveals a positive progressive
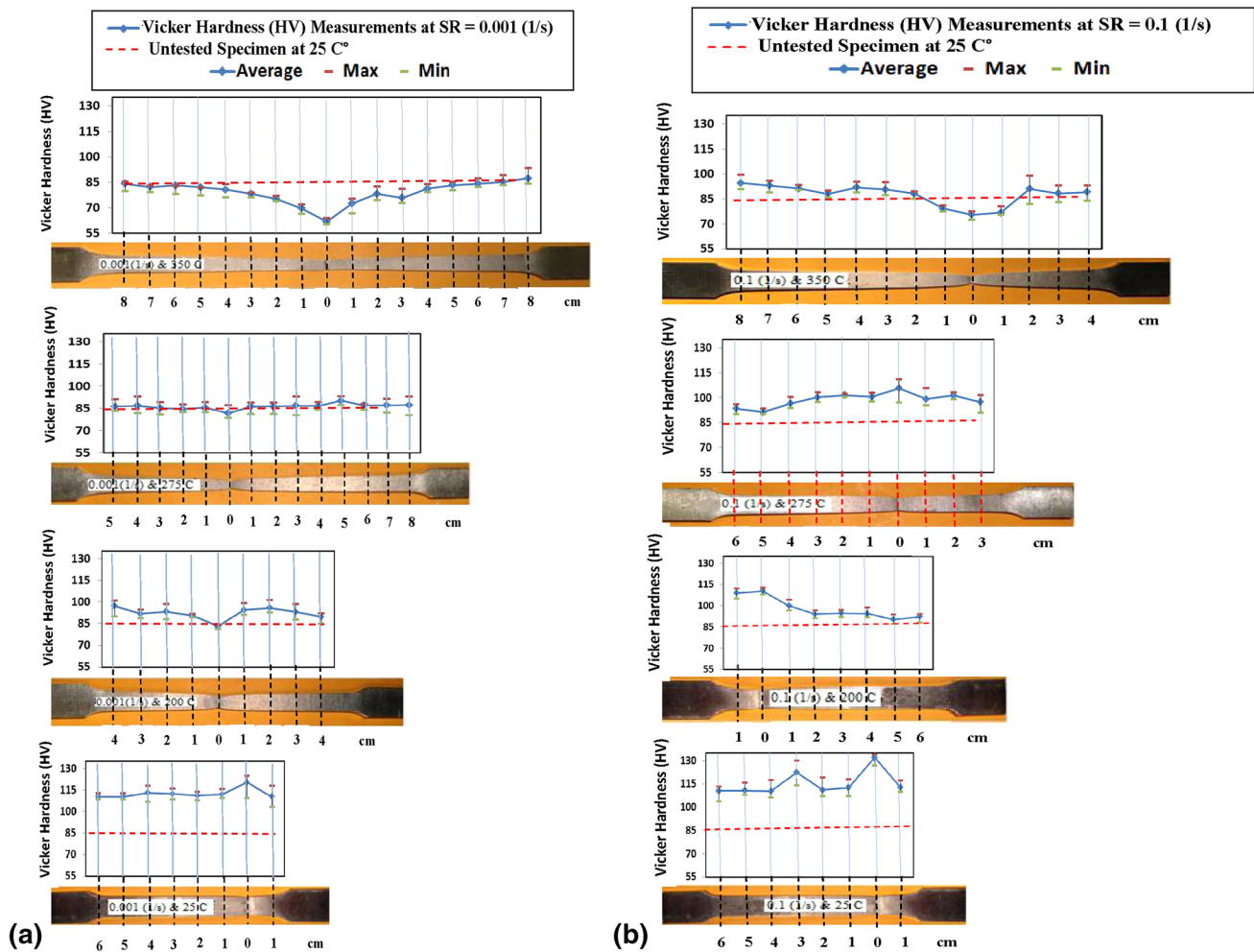
Fig. 5 Microhardness distribution along failed specimens at strain rate of (a) 0.001 s^{-1} and (b) 0.1 s^{-1}

hardening. This behavior was observed from Fig. 4(a) and (b) where the hardening modulus at 275 °C falls rapidly to zero value in the range of strain varying from 0 to 30%. Then, the modulus increases up to the ultimate tensile strength.

For a strain rate of 0.1 s^{-1} (Fig. 4b), the same remarks are valid, but with lower levels of plastic strains at fracture particularly at high temperatures as shown in Fig. 4(a).

3.2 Microhardness Analysis

Figure 5(a) and (b) illustrate microhardness profiles along deformed tensile specimens. The profiles show a uniform hardness distribution along the deformed samples except for the region where failure occurred. This observation is consistent with the uniformity of deformation achieved in all samples. Lower microhardness was observed at higher temperature and at lower strain rate. When relating the microhardness profiles to the true stress-true strain curves shown in Fig. 3(a) and (b), a clear correlation can be observed between the fracture strength of a specimen and its microhardness profile. These observations are explained based on the well-established direct relation between hardness and strength.

Figure 5(a) shows the evolution of microhardness along the specimen failed axis and points out also the effect of temperature. Based on the final length up to failure, it was observed that the superplasticity increases with the rise of

temperature under this low strain rate. For example, at a temperature of 350 °C, a recrystallization phenomenon occurs and this is accentuated in the necking zone due to the inelastic strain localization (Ref 25, 26). Such a mechanism drives a gradual decrease in the microhardness from the specimen extremities to the necking zone.

At 275 °C, a competition between the plastic strain (leading to increase the dislocation density and then increase of local hardness) and the recrystallization phenomenon induces an inelastic behavior where a similar microhardness was recorded in the tested zone compared to untested specimen. For the other two temperatures (200 and 25 °C), the microhardness trend showed a general increase, especially in the necking zone at room temperature.

Under a higher strain rate of 0.1 s^{-1} (Fig. 5(b)), the impact of the temperature becomes less important on the microhardness evolution across the specimen axis. However, the in-homogeneity of the hardness remains generally valid as it has been shown above.

3.3 Void Analysis

The area fraction of voids measurement method was used in this research to evaluate the damage which is characterized by void nucleation, growth, and coalescence in regions near the fracture surface where plastic strains and the associated stresses
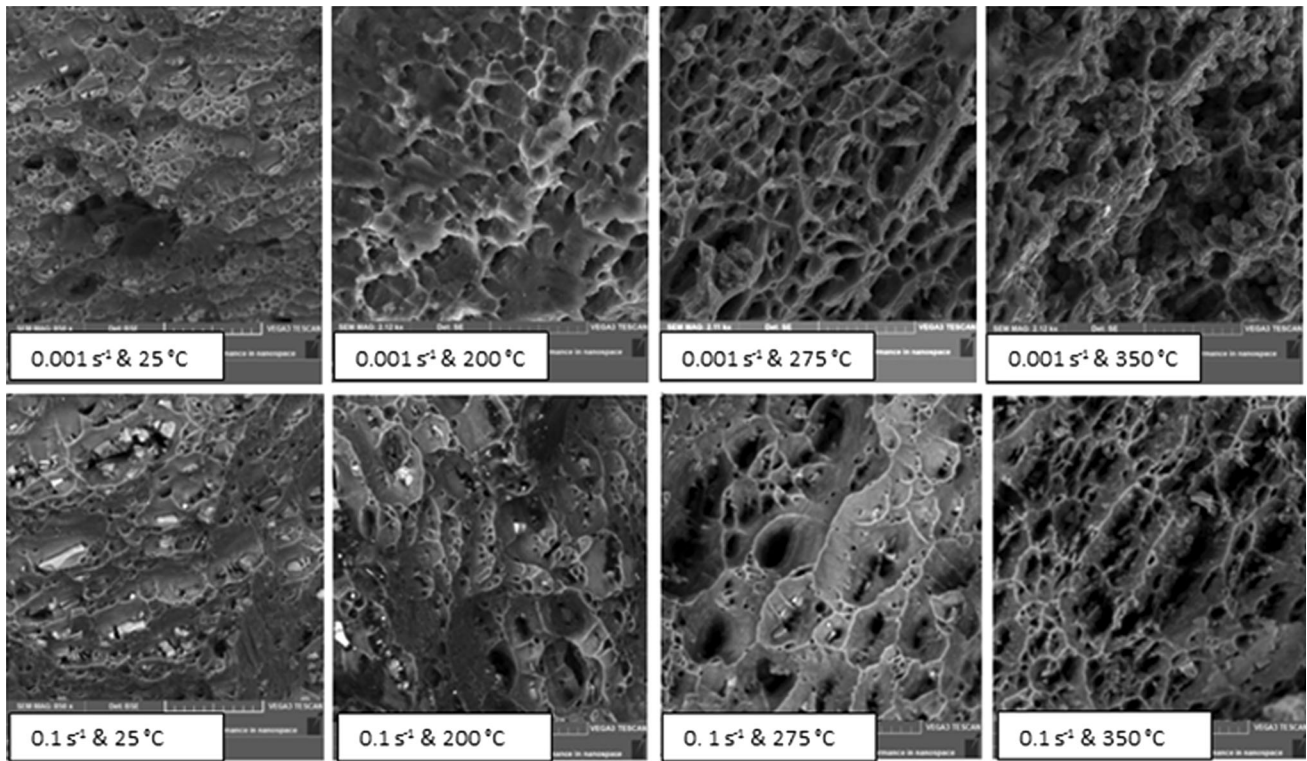
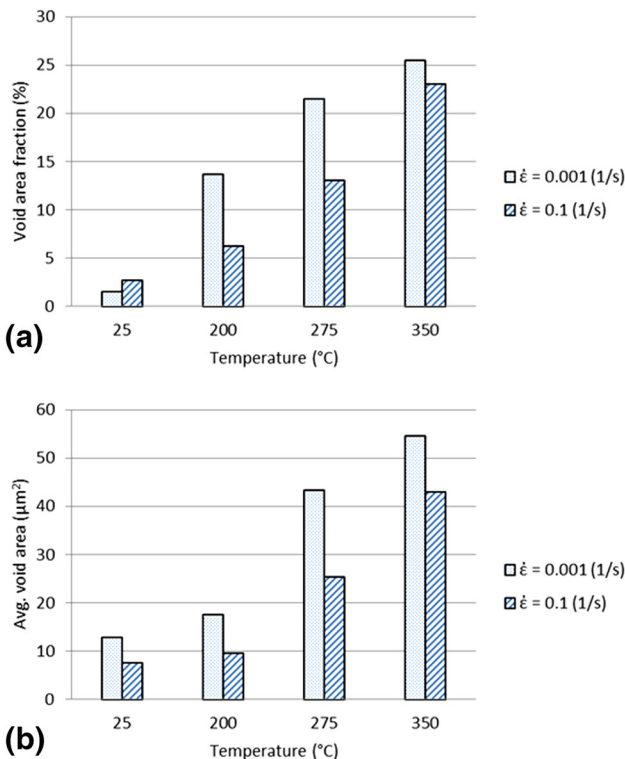**Fig. 6** SEM images for fractured surfaces

Fig. 7 (a) Void area fraction and (b) average void size

are the highest. Micrographs of fractured regions were captured using scanning electron microscopy with suitable magnifications as illustrated in Fig. 6. These micrographs show the surfaces at fracture for all tensile specimens that were loaded at different strain rates and initial temperatures.

Results for the area of void growth and coalescence obtained from fractured specimens under different load combinations are also presented in the bar chart shown in Fig. 7(a). It is obvious that void area fraction increases with increasing temperature for both strain rates. At room temperatures, the specimens deformed at higher strain rate ($0.1~\mathrm{s}^{-1}$) experienced more void area fraction as compared to the one fractured at lower rate ($0.001~\mathrm{s}^{-1}$). This suggests that damage increases with strain rate, which agrees well with previous studies (Ref 10, 27, 28). However, the bar chart presented in Fig. 7(a) shows higher void area fraction at the lower strain rate for fractured specimens deformed at higher temperatures, i.e., beyond the ambient value. This could be attributed to the fact that the 5083 aluminum alloy shows very low strain rate sensitivity at room temperature. Specimens deformed at room temperature have very close fracture strains under the two quasi-static rates. However, at higher temperature, the material becomes more sensitive to the strain rate and the total accumulative strain becomes a dominant factor in determining the void area fraction.

The average void size results for all tested specimens are also presented in Fig. 7(b), it is evident that bigger voids were formed at higher temperatures and lower strain rates; this can be explained by the combination effect of longer time available for the voids to grow at lower strain rate accompanied by the increase in fracture strain with higher temperatures.

4. Conclusion

Low ($0.001~\mathrm{s}^{-1}$) and intermediate ($0.1~\mathrm{s}^{-1}$) strain rate tensile experiments were carried out on tensile specimens extracted from

marine-grade aluminum (AA5083) sheets. The uniaxial tensile tests were conducted at four different initial temperatures (25, 200, 275, and 350 °C) to investigate the thermo-mechanical behavior and microstructure of deformed AA5083. Both yielding and hardening of AA5083 were dependent on the temperature and strain rates. Moreover, superplastic behavior was clearly observed for aluminum specimens that were tested under the low strain rate of 0.001 s^{-1} and the very high temperature of 350 °C. Void analysis was also performed in this study to investigate the microstructure of the alloy at different levels of strains, strain rates, and temperatures. Specimens were loaded to fracture and a representative element was cut from each specimen to quantify the voids fraction using SEM. The accumulation of voids and cracks depends clearly on the temperature evolution and also on the amount of plastic straining at fracture. Finally, the micro-hardness profile for each fractured specimen was examined, and then was related to its corresponding stress-strain behavior.

Acknowledgment

References

1. F. Abed, Constitutive Modeling of the Mechanical Behavior of High Strength Ferritic Steels for Static and Dynamic Applications, *Mech. Time-Depend. Mater.*, 2010, **14**, p 329–345

2. G. Voyiadjis and F. Abed, A Coupled Temperature and Strain Rate Dependent Yield Function for Dynamic Deformations of BCC Metals, *Int. J. Plast.*, 2006, **22**(8), p 1398–1431

3. F. Abed and G. Voyiadjis, A Consistent Modified Zerilli-Armstrong Flow Stress Model for BCC and FCC Metals for Elevated Temperatures, *Acta Mech.*, 2005, **175**(1–4), p 1–18

4. F. Abed and G. Voyiadjis, Thermodynamic Consistent Formulations of Viscoplastic Deformations in FCC Metals, *J. Eng. Mech.*, 2007, **133**(1), p 76–86

5. F. Abed and F. Makarem, Comparisons of Constitutive Models for Steel over a Wide Range of Temperatures and Strain Rates, *J. Eng. Mater. Technol.*, 2012, **134**(2), p 21001

6. T.G. Langdon, Fracture Processes in Superplastic Flow, *Met. Sci.*, 1982, **16**(4), p 175–183

7. J. Pilling and N. Ridley, Cavitation in Superplastic Alloys and the Effect of Hydrostatic-Pressure, *Res. Mech.*, 1988, **23**(1), p 31–63

8. N. Ridley and Z.C. Wang, Cavitation in Superplastic Metals, *Mater. Sci. Forum*, 1994, **170**, p 177–186

9. R. Kaibyshev, F. Musin, E. Avtokratova, and Y. Motohashi, Deformation Behavior of a Modified 5083 Aluminum Alloy, *Mater. Sci. Eng. A*, 2005, **392**, p 373–379

10. D.H. Bae and A.K. Ghosh, Observations Related to Healing of Interface Damage and Cavity Nucleation During Superplastic Flow, *Mater. Sci. Eng. A*, 2002, **322**, p 233–240

11. R. Vermaa, A.K. Ghosh, S. Kimb, and C. Kimb, Grain Refinement and Superplasticity in 5083 Al, *Mater. Sci. Eng. A*, 1995, **191**, p 143–150

12. S.N. Patankar and T.M. Jen, Strain Rate Insensitive Plasticity in Aluminum Alloy 5083, *Scr. Mater.*, 1998, **38**(8), p 1255–1261

13. E.A. El-Danaf, A. Almajid, and M.S. Soliman, High-Temperature Deformation and Ductility of Modified 5083 Al Alloy, *J. Mater. Eng. Perform.*, 2008, **17**, p 572–579

14. M.T. Tucker, M.F. Horstemeyer, W.R. Whittington, K.N. Solanki, and P.M. Gullett, The Effect of Varying Strain Rates and Stress States on the Plasticity, Damage, and Fracture of Aluminum Alloys, *Mech. Mater.*, 2010, **42**, p 895–907

15. R.M. Cleveland, A.K. Ghosh, and J.R. Bradley, Comparison of Superplastic Behavior in Two 5083 Aluminum Alloys, *Mater. Sci. Eng.*, 2002, **351**, p 228–236

16. H. Iwasaki, H. Hosokawa, T. Mori, T. Tagata, and K. Higashi, Quantitative Assessment of Superplastic Deformation Behavior in a Commercial 5083 Alloy, *Mater. Sci. Eng.*, 1998, **252**, p 199–202

17. M.J. Hadianfarda, R. Smerdb, S. Winklerb, and M. Worswick, Effects of Strain Rate on Mechanical Properties and Failure Mechanism of Structural Al-Mg Alloys, *Mater. Sci. Eng. A*, 2008, **492**, p 283–292

18. A.L. Gurson, Continuum Theory of Ductile Rupture by Void Nucleation and Growth: Part 1—Yield Criteria and Flow Rules for Porous Ductile Materials, *J. Eng. Mater. Technol.*, 1977, **99**, p 2–15

19. V. Tvergaard, On Localization in Ductile Materials Containing Spherical Voids, *Int. J. Fract.*, 1982, **18**, p 237–252

20. V. Tvergaard and A. Needleman, Analysis of the Cup-Cone Fracture in a Round Tensile Bar, *Acta Metall.*, 1984, **32**, p 157–169

21. F. Armero and K. Garikipati, Analysis of Strong Discontinuities in Multiplicative Finite Strain Plasticity and Their Relation with the Numerical Simulation of Strain Localization in Solids, *Int. J. Solids Struct.*, 1996, **33**, p 2863–2885

22. J. Simo, J. Oliver, and F. Armero, An Analysis of Strong Discontinuities Induced by Strain-Softening in Rate-Independent Inelastic Solids, *Comput. Mech.*, 1993, **12**, p 277–296

23. ASTM, *Standard Test Methods for Tension Testing of Metallic Materials*. ASTM E8-03, 2004

24. ASTM, *Standard Test Method for Knoop and Vickers Hardness of Materials*. ASTM E384-11, 2012

25. A. Abdul-Latif, G.F. Dirras, S. Ramtani, and A. Hocini, A New Concept for Producing Ultrafine-Grained Metallic Structures via an Intermediate Strain Rate: Experiments and Modeling, *Int. J. Mech. Sci.*, 2009, **51**, p 797–806

26. K. Zhang and H. Yan, Deformation Behavior of Fine-Grained 5083 Al Alloy at Elevated Temperature, *Trans. Nonferrous Met. Soc. China*, 2009, **19**, p 307–311

27. B. Darras, F. Abed, S. Pervaiz, and A. Abdul-Latif, Analysis of Damage in 5083 Aluminum Alloy Deformed at Different Strain Rates, *Mater. Sci. Eng. A*, 2013, **568**, p 143–149

28. F. Abed, A.K. Al-Tamimi, and R.M. Al-Himairee, Characterization and Modeling of Ductile Damage in Structural Steel at Low and Intermediate Strain Rates, *J. Eng. Mech.*, 2012, **138**(9), p 1186–1194